Low Energy K^--d Elastic Scattering: Effect of the $\bar{K}^0$-K^- and n-p Mass Differences*

J. H. HETHERINGTON† AND L. H. SCHICK‡
School of Physics, University of Minnesota, Minneapolis, Minnesota
(Received 25 August 1965)

A Faddeev type of multiple-scattering formalism with nonlocal separable S-wave potentials for the two-particle interactions is applied to K^--d scattering for incident kaon lab momentum up to 300 MeV/c. Coulomb scattering is neglected but calculations are performed both neglecting and including the $\bar{K}^0$-K^- and n-p mass differences. K^--d elastic angular distributions, elastic cross sections, and total cross sections are calculated using the Kim $\bar{K}$-N scattering lengths and values of the K^--N range parameters from 0.05 to 0.20 F. The corrections due to the mass differences run about 3–9%, being larger at the smaller values of the incident kaon momentum.

I. INTRODUCTION

IN a previous paper[1] we calculated K^--d elastic angular distributions, elastic cross sections, and total cross sections for incident-kaon laboratory momenta in the range 100–300 MeV/c. The main features of the model used in these calculations were: (a) The representation of each two-particle interaction by a nonlocal separable (NLS), S-wave, Yukawa-shaped potential[2]; (b) the neglect of Coulomb scattering; (c) the use of nonrelativistic kinematics[3]; (d) the neglect of hyperon channels, except for their contribution to the $\bar{K}$-N amplitude[4]; (e) The neglect of the $\bar{K}^0$-K^- and n-p mass splittings. With this model a Faddeev type of multiple-scattering formalism[5] was used to obtain an *exact* solution to the three-body problem.[6]

It is our aim to eventually investigate those effects which we neglected in HS1 so that our model may be made to more closely approximate the physical situation.

The primary objective of the present work was to investigate the sensitivity of the low-energy cross sections to the $\bar{K}^0$-K^- and n-p mass splittings. To this end calculations of the elastic angular distribution, elastic cross section, and total cross section for incident kaon lab momenta in the range 15–300 MeV/c were performed (a) with these mass splittings neglected, and (b) with these splittings correctly taken into account.

Aside from the inclusion of the mass splittings, the present calculations differ from those carried out in HS1 in two respects. First, as noted above we carried our calculations down to lower incident kaon momentum. Second, we used the Kim[7] values of the $\bar{K}$-N scattering lengths rather than the Humphrey-Ross[8] values.

We discuss in the next section the potentials used for the two-particle interactions. A two-channel model is used for $\bar{K}$-N scattering. The application of the Kim scattering lengths to determine the parameters of this model is covered at some length. The form of the n-p potential and its parameters are given.

In Sec. III we give the results of our 3-body calculations and look at their dependence on the mass splittings and the $\bar{K}$-N range parameter. The results obtained here are compared with some of those in HS1.

Appendices A and B contain some of the mathematical details of Sec. II and Sec. III, respectively.

II. TWO-BODY AMPLITUDES

$\bar{K}$-N scattering was taken to be a two-channel process, channel 1 being the K^-p channel and channel 2 the $\bar{K}^0n$ channel. Each element of the 2×2 matrix representing the $\bar{K}$-N "potential" was taken to be an NLS S-wave potential with a Yukawa shape.[9] The details of the calculation are given in Appendix A.

The $\bar{K}$-N input parameters were the masses of the proton, neutron, $\bar{K}^0$ and K^- (denoted by M_p, M_n, M_0, and M_-, respectively), and the isospin zero and one scattering lengths, A_0 and A_1.

* Work supported by the U. S. Atomic Energy Commission.
† Present address: Department of Physics and Astronomy, Michigan State University, East Lansing, Michigan.
‡ Present address: Department of Physics, University of Southern California, Los Angeles, California.
[1] J. H. Hetherington and L. H. Schick, Phys. Rev. **137**, B935 (1965), hereafter referred to as HS1.
[2] NLS potentials were first discussed by Y. Yamaguchi, Phys. Rev. **95**, 1628 (1954), and have been extensively applied to N-N, π-N, K-N, N-d, π-d, Λ-d, K-d, and other problems. See for example S. D. Drell and L. Verlet, Phys. Rev. **99**, 849 (1955); A. N. Mitra and V. S. Bhasin, Phys. Rev. **131**, 1265 (1963); J. H. Hetherington and L. H. Schick, Phys. Rev. **139**, B1164 (1965).
[3] For a relativistic generalization of the 3-body formalism used here, see Victor A. Alessandrini and Roland L. Omnes, Phys. Rev. **139**, B167 (1965).
[4] For a complete treatment of $\bar{K}$-N scattering including hyperon channels, Coulomb scattering, and relativistic kinematics see R. H. Dalitz, Rev. Mod. Phys. **33**, 471 (1961), and references cited there.
[5] L. D. Faddeev, Zh. Eksperim. i Teor. Fiz. **39**, 1459 (1960) [English transl.: Soviet Phys.—JETP **12**, 1014 (1961)]; Dokl. Akad. Nauk **138**, 561 (1961), **145**, 301 (1962) [English transls.: Soviet Phys.—Doklady **6**, 384 (1961), **7**, 600 (1963)]. See also C. A. Lovelace, Phys. Rev. **135**, B1225 (1964) and S. Weinberg, Phys. Rev. **133**, B232 (1964).
[6] For applications of a similar formalism to n-d scattering see R. Aaron, R. D. Amado, and Y. Y. Yam, Phys. Rev. Letters **13**, 574 (1964); V. S. Bhasin, G. L. Shrenk, and A. N. Mitra, Phys. Rev. **137**, B398 (1965).
[7] Jae Kwan Kim, Phys. Rev. Letters **14**, 29 (1965).
[8] W. R. Humphrey and R. R. Ross, Phys. Rev. **127**, 1305 (1962).
[9] Because we use only S-wave potentials, spin flip cannot occur. Thus in both the $\bar{K}$-N and K^--d problems spin coordinates may be ignored.

For the masses two different sets of values were used. In one case we took into account the $\bar{K}^0$-K^- and n-p mass splittings. In this case we used[10]

$$M_p=938.256 \text{ MeV}, \quad M_n=939.550 \text{ MeV},$$
$$M_-=493.8 \text{ MeV}, \quad M_0=498.0 \text{ MeV}. \quad (2.1)$$

The energy difference Δ between channels 1 and 2 is in this case given by

$$\Delta=5.494 \text{ MeV}. \quad (2.2)$$

With k_j the c.m. momentum in the jth channel and μ_j the reduced mass in the jth channel, we have

$$k_2=[(\mu_2/\mu_1)(k_1^2-k_0^2)]^{1/2}, \quad (2.3)$$

where k_0 is the value of k_1 at the threshold for channel 2; i.e.,

$$k_0=(\Delta/2\mu_1)^{1/2}=59.62 \text{ MeV}/c. \quad (2.4)$$

We shall refer to this case as the $\Delta\neq0$ case.

The second set of mass values was used for calculations in which we neglected the mass splittings. In this case we used[11]

$$M_n=M_p=938.9 \text{ MeV},$$
$$M_0=M_-=493.8 \text{ MeV}. \quad (2.5)$$

In this case of course $k_0=0$ and $\Delta=0$. We shall refer to this case as the $\Delta=0$ case.

For the scattering lengths we used the values given by Kim[7]

$$A_0=(-1.674+i0.722) \text{ F},$$
$$A_1=(-0.003+i0.688) \text{ F}. \quad (2.6)$$

Since Kim's results were based on a zero-effective-range model, we took as our "experimental data" the K^--p elastic, charge-exchange, and total cross sections for values of k_1 up to 300 MeV/c,[12] calculated from a zero-range R-matrix formalism[13] with the values (2.6) as input parameters. This was done for both $\Delta=0$ and $\Delta\neq0$. These "experimental" cross sections are shown in Fig. 1.

Our finite range potential model for $\bar{K}$-N scattering contained three parameters[14]; two strength parameters λ_+ and λ_- and one range parameter $1/\beta$. These parameters were handled in the following ways.

For $\Delta=0$ we used an isospin-state representation for

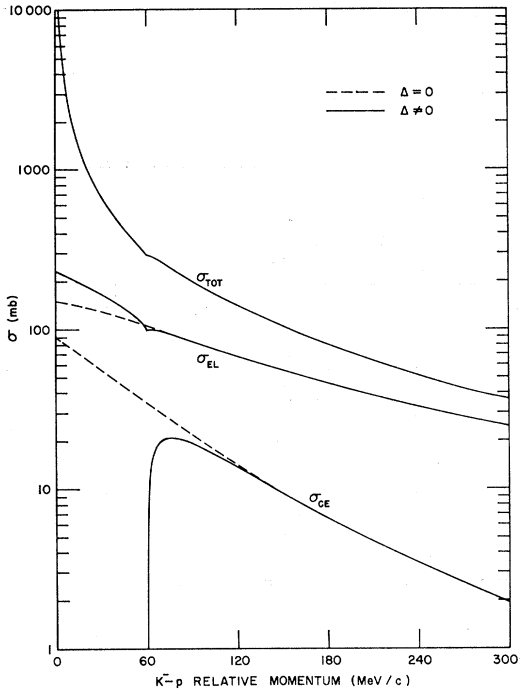

FIG. 1. Two-body cross sections plotted as a function of relative K^--p momentum. The solid curve shows the total, elastic, and charge exchange scattering cross sections as calculated from the zero-range R-matrix formulation with the Kim scattering lengths. The dashed curves show the elastic and charge exchange cross section when the mass difference is ignored. The mass difference zero curve for the total cross section lies within the solid total cross section curve except at the cusp and was not plotted.

the $\bar{K}$-N amplitudes.[15] The parameters $\lambda_1=\lambda_++\lambda_-$ and $\lambda_0=\lambda_+-\lambda_-$ were determined for a given value of β^{-1} by equating the isospin zero and one scattering lengths as calculated from our NLS potential model to the Kim values. The "given" values of β^{-1} were limited from above by the requirement that our model give a reasonable fit to the "experimental" values of the K^--p cross sections. The results listed in Table I show that for $\beta^{-1}\lesssim0.2$ F we have a fairly good fit. From calculations performed in HS1 we found that in order to obtain an accurate solution to the 3-body problem on the computer available to us without using very fancy numerical techniques, we had to take $\beta^{-1}\gtrsim0.05$ F. Most of our calculations (for both $\Delta=0$ and $\Delta\neq0$) were carried out therefore at $\beta^{-1}=0.10$ F. The range dependence of our results was investigated by repeating some calculations with $\beta^{-1}=0.05$ F and $\beta^{-1}=0.20$ F.

For $\Delta\neq0$ two different fits were used to determine λ_+ and λ_- for a given value of β^{-1}. In fit No. 1 we matched the $K^-p\to K^-p$ amplitude at its threshold ($k_1=0$) and the $K^-p\to\bar{K}^0n$ amplitude at its threshold ($k_1=59.62$ MeV/c) to their "experimental" values.[16]

[10] Arthur H. Rosenfeld, Angela Barbaro-Galtieri, Walter H. Barkas, Pierre L. Bastien, Janos Kirz, and Mittis Roos, Rev. Mod. Phys. **36**, 977 (1964).

[11] The nucleon mass is just the average of M_n and M_p given in Eq. (2.4). This value and the K^- value for the kaon mass were used in HS1. These values were used here for $\Delta=0$ in order to facilitate comparison with the HS1 results.

[12] Values of the K^--p relative momentum above this upper limit do not contribute significantly to the K^--d cross sections. This also indicates that our use of nonrelativistic kinematics throughout is at least a consistent procedure.

[13] For a nonrelativistic zero-range R-matrix treatment of K^--p scattering see J. D. Jackson and H. W. Wyld Jr., Nuovo Cimento **13**, 85 (1959).

[14] See Appendix A.

[15] This representation may be obtained from the charge-state representation of Appendix A for $\Delta=0$ by diagonalization.

[16] The "experimental" values of the amplitudes are just those which yield the "experimental" cross sections shown in Fig. 1.

TABLE I. K^--p elastic, charge exchange, and total cross sections in millibarns as functions of the K^--p relative momentum. The $\bar{K}^0$-K^- and n-p mass splittings have been ignored. Column 3 follows from a zero range R-matrix calculation, and columns 4, 5, and 6 from an NLS potential calculation with different ranges. All four calculations fit the Kim scattering lengths at zero K^--p relative momentum.

Cross section	K^--p relative momentum (MeV/c)	Zero-range R matrix	$\beta^{-1}=0.05$	$\beta^{-1}=0.10$	$\beta^{-1}=0.20$
σ_{el}	10	145.1	145.1	145.2	145.3
	60	105.6	106.6	107.5	108.9
	160	51.89	53.21	54.12	54.73
	260	29.48	30.26	30.46	29.21
σ_{ce}	10	75.75	75.80	75.84	75.91
	60	34.37	34.81	35.22	35.95
	160	8.301	8.608	8.898	9.413
	260	2.784	2.919	3.041	3.247
σ_{tot}	10	1845.	1845.	1846.	1847.
	60	322.6	325.2	327.5	331.4
	160	95.00	97.09	98.71	100.5
	260	45.25	46.36	46.82	45.94

In fit No. 2 we matched both of these amplitudes to their respective "experimental" values at the charge exchange threshold. Fit No. 1 was calculated for $\beta^{-1}=0.05$, 0.10, and 0.20 F while fit No. 2 was calculated for $\beta^{-1}=0.1$ F.

The results of these $\Delta\neq 0$ calculations for some typical values of k_1 are shown in Table II. It is clear from this table that for $0.05\text{ F}\lesssim\beta^{-1}\lesssim 0.20\text{ F}$ the range-dependence of the cross sections is quite small, but that for $\beta^{-1}>0.20$ F this range dependence would become appreciable. Furthermore, both fit No. 1 and fit No. 2 reproduce the momentum dependence of the "experimental" cross sections quite well. Although fit No. 2 may be slightly better in terms of a least-squares fit to the "experimental" cross sections, fit No. 1 is the better fit in the low-momentum region. As this low momentum region is the more important in the 3-body calculation, we chose to perform most of our 3-body calculations with the $\bar{K}$-N parameters determined by fit No. 1.

In Table III we list the values of λ_+ and λ_- as

TABLE II. K^--p elastic, change exchange, and total cross sections in millibarns as functions of the K^--p relative momentum for various fits to the Kim scattering lengths. The $\bar{K}^0$-K^- and n-p mass splittings have been correctly taken into account.

Cross section	K^--p relative momentum (MeV/c)	Zero-range R matrix	Fit No. 1 $\beta^{-1}=0.05$	Fit No. 1 $\beta^{-1}=0.10$	Fit No. 1 $\beta^{-1}=0.20$	Fit No. 2 $\beta^{-1}=0.10$
σ_{el}	10	210.5	210.6	210.7	211.0	202.0
	60	99.35	100.8	102.8	106.0	99.38
	160	52.01	53.44	55.03	56.66	53.83
	260	29.51	30.24	30.81	30.03	30.30
σ_{ce}	60	6.028	6.051	6.036	6.027	6.048
	160	8.286	8.805	8.745	8.880	9.103
	260	2.800	3.026	3.005	3.055	3.172
σ_{tot}	10	2012.	2013.	2015.	2017.	1938.
	60	292.7	297.2	301.1	308.2	292.8
	160	94.93	97.29	99.44	102.2	98.15
	260	45.27	46.37	47.09	46.59	46.68

TABLE III. The $\bar{K}$-N potential parameters λ_+ and λ_- (in units of $(2\pi)^3\times 10^6$ MeV^2) for the cases studied.

	$\beta^{-1}=0.05$ F	$\beta^{-1}=0.10$ F	$\beta^{-1}=0.20$ F
		$\Delta=0$	
λ_+	$-9.7790-i0.8016$	$-1.2224-i0.1938$	$-0.1493\ -i0.04292$
λ_-	$+0.3492-i0.5699$	$+0.1121-i0.1294$	$+0.03679-i0.02267$
		$\Delta\neq 0$ Fit No. 1	
λ_+	$-9.7649-i0.8173$	$-1.2240-i0.1933$	$-0.1510\ -i0.04286$
λ_-	$+0.3370-i0.5962$	$+0.1065-i0.1308$	$+0.03427-i0.02324$
		$\Delta\neq 0$ Fit No. 2	
λ_+		$-1.2209-i0.1987$	
λ_-		$+0.1124-i0.1365$	

determined by the $\Delta=0$ and the $\Delta\neq 0$ fit No. 1 and fit No. 2 calculations.

The other two-particle potential that enters the K^--d problem is the $^3S_1$ nucleon-nucleon potential. This potential too was taken to be an NLS potential with a Yukawa shape. The values of the parameters in this potential were taken from Yamaguchi. In terms of the inverse of the range parameter β_N and the inverse of the size of the deuteron α, where $\alpha^2=[2M_pM_nB/(M_n+M_p)]$ with $B=2.225$ MeV, these values are

$$\alpha=45.706\text{ MeV}/c,$$
$$\beta_N=6.255\alpha. \tag{2.7}$$

The strength of the potential λ_N is related to these parameters by

$$\lambda_N=-4\pi\beta_N(\alpha+\beta_N)^2(M_n+M_p)/M_nM_p. \tag{2.8}$$

III. RESULTS OF THE K^--d CALCULATIONS

In HS1 we used a Faddeev type of multiple scattering formalism and NLS S-wave potentials for the two-particle interactions to reduce the problem of finding the K^--d elastic scattering amplitude (with $\Delta=0$) to that of solving a set of three coupled one-dimensional integral equations for each partial wave. The kernels of these equations were singular but by judicious use of

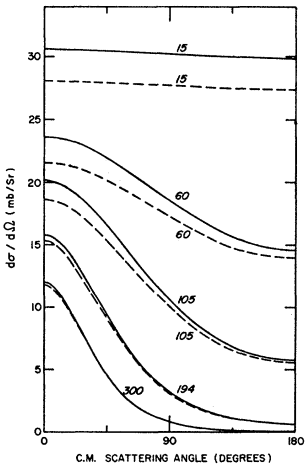

FIG. 2. Elastic differential cross section for K^--d scattering for various values of the laboratory K^- momentum. The dashed curves are for the case $\Delta=0$, the solid curves for the case $\Delta\neq 0$. In both cases $\beta^{-1}=0.1$F.

TABLE IV. K^--d elastic and total cross sections in millibarns as functions of the incident-kaon lab momentum for various sets of $\bar{K}$-N parameters.

Cross section	K^- lab momentum (MeV/c)	$\Delta=0$ $\beta^{-1}=0.05$ F	$\Delta=0$ $\beta^{-1}=0.10$ F	$\Delta=0$ $\beta^{-1}=0.20$ F	$\Delta\neq0$ Fit No. 1 $\beta^{-1}=0.05$ F	$\Delta\neq0$ Fit No. 1 $\beta^{-1}=0.10$ F	$\Delta\neq0$ Fit No. 1 $\beta^{-1}=0.20$ F	$\Delta\neq0$ Fit No. 2 $\beta^{-1}=0.10$ F
σ_{el}	15	356	348	352	391	380	382	371
	60	221	219	226	238	235	242	231
	150	83.5	84.2	88.4	86.6	88.0	93.2	86.7
	250	34.7	35.1	36.1	34.9	35.9	37.6	35.2
σ_{tot}	15	2450	2370	2290	2600	2500	2400	2450
	60	653	642	641	688	677	675	665
	150	261	261	266	263	267	274	262
	250	143	144	146	143	145	149	143

contour integration and analytic continuation we could get around these singularities. The set of coupled integral equations was then solved on the CDC 1604 at the University of Minnesota Numerical Analysis Center.[17]

In the present work our $\Delta=0$ K^--d calculations used exactly the same equations given in HS1 but with the Kim values, rather than the Humphrey-Ross values, of the $\bar{K}$-N scattering lengths. For our $\Delta\neq0$ K^--d calculations in the present work we used the same 3-body formalism,[18] mathematical analysis, and numerical techniques as were used previously. A sketch of the derivation is given in Appendix B.

As before we calculated the elastic angular distribution, elastic cross section, and total cross section for a range of initial kaon lab momenta p_0 and with various values for the two-body input parameters. The values of p_0 used here were[19] $p_0=15$, 60, 105, 150, 194, 250, and 300 MeV/c. The values used for the two-body parameters were those discussed in Sec. II. Our results are displayed in Figs. 2, 3, and 4 and Table IV.

In Fig. 2 we have plotted the K^--d elastic angular distributions for $p_0=15$, 60, 105, 194, and 300 MeV/c. We obtained the solid line curves by using the $\Delta\neq0$, fit No. 1, $\beta^{-1}=0.1$ parameters of Table III. We obtained the dashed curves by using the same range but with $\Delta=0$.

In Fig. 3 we have plotted the K^--d elastic and total cross sections (σ_{el} and σ_{tot}, respectively) as functions of the incident-kaon lab momentum for the $\Delta\neq0$, fit No. 1, $\beta^{-1}=0.1$, and the $\Delta=0$, $\beta^{-1}=0.1$ sets of parameters.

How σ_{el} and σ_{tot} depend upon β^{-1}, upon whether $\Delta=0$ or $\Delta\neq0$, and (if $\Delta\neq0$) upon the choice of fit No. 1 or fit No. 2 input parameters is shown in Table IV.

As a further look at the sensitivity of the K^--d σ_{el} and

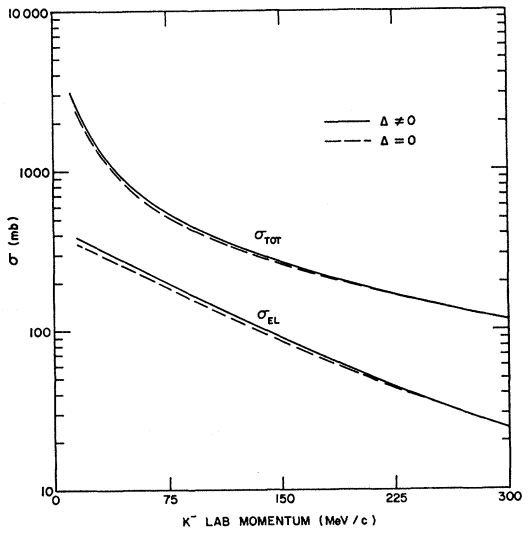

FIG. 3. Elastic and total cross sections for K^--d scattering as functions of K^- laboratory momentum, for the $\Delta=0$ and $\Delta\neq0$ cases. The range parameter β^{-1} was taken to be 0.1F.

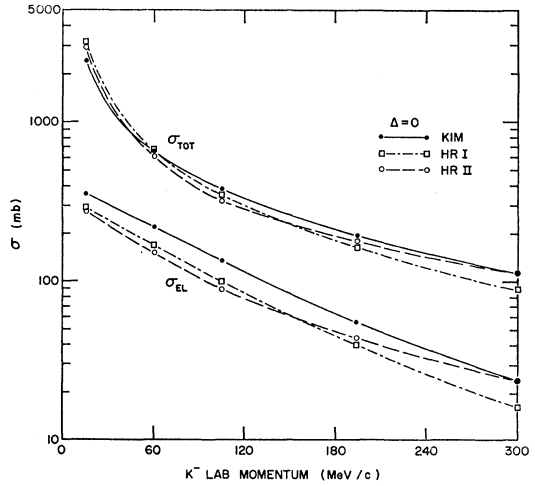

FIG. 4. The total and elastic K^--d cross sections corresponding to the Kim, Humphrey-Ross I, and Humphrey-Ross II sets of two-body scattering lengths. In all cases the mass difference was ignored and the range parameter β^{-1} was taken to be 0.1F.

[17] All computations in this work were also done on this machine. The numerical analysis was carried out so as to maintain an accuracy of 1% in all results.

[18] With $\Delta\neq0$ isospin is not a good quantum number so that a charge state representation had to be used in place of the isospin-state representation of HS1.

[19] In terms of p_0 the $K^-+d\rightarrow K^-+n+p$ threshold occurs at 52.7 MeV/c and the $K^-+d\rightarrow\bar{K}^0+n+n$ threshold occurs at 98.1 MeV/c.

σ_{tot} to the $\bar{K}$-N parameters we have plotted in Fig. 4 these cross sections as functions of incident kaon lab momentum for three different sets of these parameters. In each of these sets we used $\Delta=0$ and $\beta^{-1}=0.1$, but in one set we used the Kim scattering lengths, in another the Humphrey-Ross set I (HRI) scattering lengths, and in the third the Humphrey-Ross set II (HRII) scattering lengths.[20]

The main features of these results are:

(i) The difference in the K^--d cross sections for the two $\Delta\neq 0$ sets of $\bar{K}$-N parameters is quite small ($\simeq 2\%$). For the values of β^{-1} considered the variation in the size of the cross sections is also only one or two percent. These results indicate that any set of $\bar{K}$-N parameters that give a good fit to the low-energy K^--p scattering data will also give a good fit to the low-energy, elastic, K^--d cross sections.

(ii) The neglect of the $\bar{K}^0$-K^- and n-p mass splittings leads at worst (i.e., at $p_0=15$ MeV/c) to an error in the K^--d cross sections studied of about 9%. At $p_0=100$ MeV/c this error is down to about 5% and for $p_0\gtrsim 250$ MeV/c it becomes comparable to the other small uncertainties in the calculation.

(iii) For σ_{el} the difference between the calculations using the Kim data and those using the Humphrey-Ross data is $\simeq 15\%$ for $p_0\lesssim 200$ MeV/c. In the near future experimental results for the K^--d elastic plus breakup cross sections in the range $p_0=100$–300 MeV/c accurate to 5% will become available.[21] If the breakup cross section dependence on the $\bar{K}$-N scattering lengths doesn't compensate for the dependence of σ_{el} on these parameters, then at least sets of scattering lengths as different as the Kim and Humphrey-Ross sets will lead to measurably different K^--d cross sections.[22]

APPENDIX A

The Lippman-Schwinger equation for t, the $\bar{K}$-N t matrix, was taken to be

$$t=V+Vgt, \tag{A1}$$

with the t matrix, the potential V, and the Green's function g given by

$$t=\begin{pmatrix} t_{11} & t_{12} \\ t_{21} & t_{22} \end{pmatrix}, \quad V=\begin{pmatrix} V_{11} & V_{12} \\ V_{21} & V_{11} \end{pmatrix}, \tag{A2}$$

$$g=\begin{pmatrix} g_1 & 0 \\ 0 & g_2 \end{pmatrix}, \tag{A3}$$

respectively. Here row (column) one refers to the K^-p channel and row (column) two to the $\bar{K}^0n$ channel. The energy variable that labels both t and g has been suppressed, but it should be remembered that g_1 describes the free propagation of a K^- and a proton at a c.m. energy E_1 while g_2 describes the free propagation of a $\bar{K}^0$ and a neutron at a c.m. energy $E_2=E_1-\Delta$.

Each element of the matrix V was taken to have a NLS S-wave form. With r_i (r_j') the interparticle distance in the final (initial) state, we used

$$\langle r_i|V_{ij}|r_j'\rangle=\lambda_{ij}v_i(r_i)v_j(r_j'), \tag{A4}$$

with

$$\begin{aligned}\lambda_{ij}&=\lambda_+, \quad i=j \\ &=\lambda_-, \quad i\neq j.\end{aligned} \tag{A5}$$

(Were isospin a good quantum number, we would have $\lambda_\pm=\frac{1}{2}(\lambda_1\pm\lambda_0)$ with λ_j the potential strength for isospin j.) The shapes $v_i(r)$ were taken to be the same for both channels, namely

$$v_i(r)=(4\pi r)^{-1}\exp(-\beta r). \tag{A6}$$

This gave us three parameters (λ_+, λ_-, and β) to be determined from the two experimentally known scattering lengths A_0 and A_1.

With Eqs. (A4), (A5), and (A6), Eq. (A1) was solved exactly. If we let $\langle k_i|t_{ij}|k_j'\rangle$ denote the t matrix element for scattering from a state in channel j of relative momentum k_j' to a state in channel i of relative momentum k_i, then the solution to Eq. (A1) may be written

$$\langle k_i|t_{ij}|k_j'\rangle=v_i(k_i)\tau_{ij}v_j(k_j'), \tag{A7}$$

with

$$\tau_{11}=[\lambda_+(1-\bar{g}_2\lambda_+)+\lambda_-^2\bar{g}_2]/D, \tag{A8}$$

$$\tau_{22}=[\lambda_+(1-\bar{g}_1\lambda_+)+\lambda_-^2\bar{g}_1]/D, \tag{A9}$$

$$\tau_{12}=\lambda_-/D=\tau_{21}, \tag{A10}$$

$$D=(1-\bar{g}_1\lambda_+)(1-\bar{g}_2\lambda_-)-\bar{g}_1\bar{g}_2\lambda_-^2, \tag{A11}$$

$$\bar{g}_i=-(\mu_i/4\pi)[\beta(\beta-ik_i)]^{-1}. \tag{A12}$$

For K^--p scattering the elastic, total, and charge-exchange cross sections are given by

$$\sigma_{\text{el}}=\pi k_1^{-2}|\langle k_1|t_{11}|k_1\rangle|^2, \tag{A13}$$

$$\sigma_{\text{tot}}=2\pi k_1^{-2}\text{Im}\langle k_1|t_{11}|k_1\rangle, \tag{A14}$$

$$\sigma_{\text{ce}}=\pi k_1^{-2}|\langle k_2|t_{21}|k_1\rangle|^2. \tag{A15}$$

The "experimental" amplitudes, i.e., the zero-effective-range amplitudes were taken to be[13]

$$\langle k_1|t_{11}|k_1\rangle=[2k_1k_2(A_-^2-A_+^2)-2ik_1A_+]/D_0, \tag{A16}$$

$$\langle k_2|t_{21}|k_1\rangle=-2iA_-(k_1k_2)^{1/2}/D_0, \tag{A17}$$

where

$$D_0^{-1}=1+k_1k_2(A_-^2-A_+^2)-iA_+(k_1+k_2), \tag{A18}$$

$$A_\pm=\tfrac{1}{2}(A_1\pm A_0). \tag{A19}$$

The "experimental" K^--p cross sections are the result of using Eqs. (A16) and (A17) in Eqs. (A13), (A14), and (A15) with the Kim values of A_0 and A_1.

[20] From Ref. 8 we have for HRI, $A_0=(-0.22+i2.74)$F and $A_1=(0.02+i0.38)$F, while for HRII, $A_0=(0.59+i0.96)$F and $A_1=(1.20+0.56)$F.

[21] R. D. Hill (private communication).

[22] Calculations of this cross section are in progress. The sensitivity of the results to the model assumed for the neutron-proton interaction will also be investigated.

APPENDIX B

There are only three particles present at any one time in the scattering process, so that the Faddeev type of multiple-scattering equations used in HS1 could also be used here. Thus the matrix element for elastic scattering is given by

$$M_{ba}=\sum_{i,j\neq 2}\langle\phi_b{}^i|T^{ij}|\phi_a{}^j\rangle, \tag{B1}$$

with

$$T^{ij}=\hat{t}_i\delta_{ij}+\sum_{k=1}^{3}\hat{t}_i\hat{G}^{ik}T^{kj}, \tag{B2}$$

$$\hat{t}_i=V_i[1-GV_i]^{-1}, \tag{B3}$$

$$\hat{G}^{ik}=G(1-\delta_{ik}), \tag{B4}$$

where $\phi_b{}^i$ ($\phi_a{}^j$) is the final (initial) wave function for a deuteron and a plane wave K^- expressed in the ith (jth) "natural" coordinate system discussed in HS1, and G is the three-body free particle Green's function.[23]

In the present work, however, each of the $\hat{t}_j$ is an operator in the subspace whose states are defined in Table V. With row (column) j referring to state j, the matrices representing the $\hat{t}_i$ are

$$\hat{t}_1=\begin{bmatrix} t_1 & t_2 & 0 \\ \tilde{t}_2 & t_3 & 0 \\ 0 & 0 & t_4 \end{bmatrix}, \tag{B5}$$

$$\hat{t}_2=\tfrac{1}{2}\begin{bmatrix} t_0 & 0 & -t_0 \\ 0 & 0 & 0 \\ -t_0 & 0 & t_0 \end{bmatrix}, \tag{B6}$$

$$\hat{t}_3=\begin{bmatrix} t_4 & 0 & 0 \\ 0 & t_3 & \tilde{t}_2 \\ 0 & t_2 & t_1 \end{bmatrix}, \tag{B7}$$

where the reactions represented by each of the t-matrices t_i, $i=0, \cdots, 4$ are given in Table VI.[24]

The Green's functions $\hat{G}^{ik}$ are also operators in this subspace, but they are diagonal. Through their dependence on the particle masses and the total kinetic energy, the $\hat{G}^{ik}$ are also state-dependent;

$$\hat{G}^{ik}=\begin{bmatrix} G_1{}^{ik} & 0 & 0 \\ 0 & G_2{}^{ik} & 0 \\ 0 & 0 & G_3{}^{ik} \end{bmatrix}, \tag{B8}$$

where the subscript denotes the state.

Similarly, $\phi_a{}^j$ may be written as a vector in this 3-space. Since the deuteron is in an isospin-zero state we have,

$$\phi_a{}^j=\tfrac{1}{2}\sqrt{2}\begin{bmatrix} \psi_{a1}{}^j \\ 0 \\ -\psi_{a3}{}^j \end{bmatrix}, \tag{B9}$$

where $\psi_{ai}{}^j$ is the spatial part of the initial wave functions in the jth "natural" coordinate systems and the ith state of Table V.

The scattering matrix element can now be written

$$M_{ba}=\tilde{\Phi}_b(\hat{t}+\hat{t}\mathcal{G}\hat{t})\Phi_a, \tag{B10}$$

where

$$\mathcal{G}=\hat{G}+\hat{G}\hat{t}\mathcal{G}. \tag{B11}$$

Here Φ_a is the nine-element column matrix made from $\phi_a{}^1$, $\phi_a{}^2\equiv 0$, $\phi_a{}^3$, $\hat{t}$ is the 9×9 matrix made up of the three $\hat{t}_i$'s along its diagonal, and $\hat{G}$ is the 9×9 off-diagonal matrix of the G^{ik}. Because there are only four different "interactions" (t_0, t_4, and the 2×2 $\bar{K}$-N charge zero interaction) these 9×9 matrix equations may be reduced to 4×4 matrix equations. That is, Eqs. (B10) and (B11) still hold, but with

$$\Phi_a=\begin{bmatrix} 0 \\ \psi_{a1}{}^3 \\ 0 \\ -\psi_{a3}{}^3 \end{bmatrix},$$

$$\hat{t}=\begin{bmatrix} t_0 & 0 & 0 & 0 \\ 0 & t_4 & 0 & 0 \\ 0 & 0 & t_3 & \tilde{t}_2 \\ 0 & 0 & t_2 & t_1 \end{bmatrix},$$

$$\hat{G}=\begin{bmatrix} 0 & A & 0 & -B \\ \tilde{A} & 0 & 0 & -C \\ 0 & 0 & -D & 0 \\ -\tilde{B} & -\tilde{C} & 0 & 0 \end{bmatrix},$$

TABLE V. Particle labels.

State No.	Particle No. 1	Particle No. 2	Particle No. 3
1	n	K^-	p
2	n	$\bar{K}^0$	n
3	p	K^-	n

TABLE VI. Reactions represented by the various two-body t matrices.

Operator	Reaction
t_0	$N+N\rightarrow N+N$ (isospin zero, $^3S_1$)
t_1	$K^-+p\rightarrow K^-+p$
t_2	$K^-+p\rightarrow \bar{K}^0+n$
$\tilde{t}_2$	$\bar{K}^0+n\rightarrow K^-+p$
t_3	$\bar{K}^0+n\rightarrow \bar{K}^0+n$
t_4	$K^-+n\rightarrow K^-+n$

[23] The energy dependence of the operators has been suppressed.

[24] The operator t_0 is the isospin-zero nucleon-nucleon scattering matrix in the $^3S_1$ state. There is no neutron-neutron scattering in this state so that the center element of $\hat{t}_2$ vanishes. The other zero elements in $\hat{t}_1$, $\hat{t}_2$, and $\hat{t}_3$ result from charge conservation in each two-particle scattering.

where

$$A=G_1^{23}=G_3^{21},$$
$$B=G_1^{21}=G_3^{23},$$
$$C=G_1^{31}=G_3^{13},$$
$$D=G_2^{13}=G_2^{31}.$$

Advantage may now be taken of the factorable nature of the interactions t_i and a partial-wave separation of these equations carried out. From this point the derivation of the set of four coupled one-dimensional integral equations for each partial wave proceeds exactly as in HS1.

PHYSICAL REVIEW VOLUME 141, NUMBER 4 JANUARY 1966

Photodisintegration of the Deuteron from 500 to 1000 MeV*

R. CHING† AND C. SCHAERF‡
High-Energy Physics Laboratory, Stanford University, Stanford, California
(Received 26 July 1965)

The photodisintegration of the deuteron has been studied at energies comparable with the second and third pion-nucleon isobars using the Stanford Mark III linear electron accelerator. No evidence has been found for any resonant behavior in the energy region of interest.

EXPERIMENTAL PROCEDURE

WE have measured the angle and momentum of the protons produced in the reaction

$$\gamma+d\rightarrow p+n,$$

using the double-focusing magnetic spectrometer of Hofstadter's group.

The same experimental apparatus and data-handling technique described in Ref. 1 has been used. The lower counting rate of this experiment required some increase in the shielding around the counters in order to reduce the accidental coincidence rate to a tolerable level. In this way the accidental coincidence rate was reduced to less than one-third of the true rate for $\theta_p^{\text{c.m.}}=130°$ and to less than $\frac{1}{10}$ for $\theta_p^{\text{c.m.}}=90°$. Two cells were filled, respectively, with liquid deuterium (full target) and with liquid hydrogen (empty target).

The emission of protons from liquid hydrogen at the angle and with the momentum accepted by our spectrometer was forbidden by kinematics for all of our points. However, the proton yield from a liquid-hydrogen target was slightly higher than the comparable yield from an empty target. We have interpreted this phenomenon as the result of two-step processes. As an example we can consider pion photoproduction in the target's walls followed by pion-nucleon scattering in the target.[2] For this reason we have assumed that the proton yield from a liquid-hydrogen target was a better approximation of the background processes contributing to our full target counting rate, than the yield from a true empty target. In these conditions the yield from the hydrogen target was comparable with the photo

TABLE I. Center-of-mass differential cross section in microbarns/steradian as a function of the gamma-ray energy k and the proton angle $\theta_p^{\text{c.m.}}$ in the c.m. system.

k (MeV)	$\theta_p^{\text{c.m.}}$ (degree)	$d\sigma/d\Omega$ (μb/sr)
975	130	0.0343±0.0133
950	130	0.0356±0.0134
925	130	0.0547±0.0143
900	130	0.0442±0.0108
850	130	0.0347±0.0118
800	130	0.0755±0.0145
975	90	0.0681±0.0093
950	90	0.0488±0.0075
925	90	0.0543±0.0089
900	90	0.0688±0.0107
875	90	0.1038±0.0082
850	90	0.1235±0.0068
825	90	0.1483±0.0096
800	90	0.1571±0.0080
775	90	0.1935±0.0164
750	90	0.2643±0.0177
725	90	0.2984±0.0197
700	90	0.3374±0.0206
675	90	0.3908±0.0238
650	90	0.3948±0.0175
625	90	0.5620±0.0210
600	90	0.5822±0.0367
575	90	0.6900±0.0280
550	90	0.6860±0.0412
525	90	0.8021±0.0441
800	137	0.0678±0.0098
800	120	0.1144±0.0128
800	110	0.1323±0.0149
800	100	0.1360±0.0166
800	80	0.1948±0.0138
800	70	0.2040±0.0151

* Work supported in part by the U. S. Office of Naval Research, Contract Nonr 225(67).
† Present address: Department of Physics, William Marsh Rice University, Houston, Texas.
‡ Present address: Laboratori Nazionali di Frascati, Frascati (ROMA), Italy.
[1] H. De Staebler, E. Erickson, A. C. Hearn, and C. Schaerf, Phys. Rev. **140**, B336 (1965).
[2] The kinematical conditions of the experiment prevented contributions from all two-step processes involving stationary nucleons.